AB INITIO STUDIES OF STRUCTURAL, ELECTRONIC, OPTICAL, ELASTIC AND THERMAL PROPERTIES OF COPPER THALLIUM DICHALCOGENIDES (CuTiX$_2$: X=S, Se, Te)

S. TOMAR[a], R. GAUTAM[b], PRAVESH[b], C. M. S. NEGI[c], S. K. GUPTA[a], S. R. BHARDWAJ[d], A. S. VERMA[a,*]
[a]*Department of Physics, Banasthali Vidyapith, Rajasthan 304022, India*
[b]*Department of Electronics and Communication Engineering, KIET Group of Institutions, Ghaziabad, 201206, India*
[c]*Department of Electronics, Banasthali Vidyapith, Rajasthan 304022, India*
[d]*Department of Physics, B. S. A. College, Mathura 281004,India*

The ground state structural, electronic, optical, elastic and thermal properties of the copper thallium chalcogenides (CuTlX$_2$: X=S, Se, Te) in the body centered tetragonal (BCT) phase have been studied using the accurate full potential linearized augmented plane wave (FP-LAPW) method. We have reported the electronic and optical properties with the recently developed density functional theory of Tran and Blaha and this theory are used along with the Wu-Cohen generalized gradient approximation (WC-GGA) for the exchange-correlation potential. Furthermore, optical features such as dielectric functions, refractive indices, extinction coefficient, optical reflectivity, absorption coefficients, optical conductivities, were calculated for photon energies up to 40 eV. The elastic constants at equilibrium in BCT structure are also determined. The thermodynamical properties such as thermal expansion, heat capacity, Debye temperature, entropy, Gruneisen parameter and bulk modulus were calculated employing the quasi-harmonic Debye model at different temperatures and pressures and the silent results were interpreted. Hardness of the materials was calculated for the first time at different temperatures and pressures.
PACS: 31.15.A-; 46.70.-P; 62.20.D-; 62.20.de; 65.40.De; 65.40.-b ; 65.60.+a ;71.20.-b

1. Introduction

There is currently a lot of interest in the science and potential technological applications of the series of compounds belonging to the A^{I}B^{III}C$_2^{VI}$ semiconductors family, where Cu is involved as a group I element. These materials normally crystallize in chalcopyrite structure, which is a super lattice of the cubic zinc-blende structure. The symmetry of the structure is lowered and therefore it is no longer cubic but tetragonal with the lattice parameters ratio (c/a) equal to or, in most of the cases, slightly less than 2 [1-7]. Cu-chalcopyrites have been attracting attention as potential materials for next-generation electro-optical and spin-electronics devices. These materials the most promising semiconductors with chalcopyrite structure used in the absorber layer of thin-film solar cells. Chalcopyrite based solar cells are becoming leading technologies for solar energy generators being champions in terms of efficiency (which is about 20%) among thin-film devices [8,9]. One of their mysterious features is super high tolerance to any radiation. Their life-time in outer space was found to be at least 50 times as long as that of amorphous silicon solar cells. In fact, irradiation with quite high doses of MeV protons and electrons improves their performance. The material seems to repair itself at room temperature. Despite such achievements very little is known about these materials in comparison with Si or binary compounds. To make

---

*Corresponding author: ajay_phy@rediffmail.com

the design of solar cells more scientific we have to learn more about the defects in the chalcopyrites [6-9].

The development of the computational methods has led a new class of first principle's approaches. The complexities of experiments are removed as only the atomic numbers of the constituent atoms are required inputs. We found that the structural, electronic, optical, elastic and thermodynamic study have never been done by ab initio calculation for these compounds. Therefore in this paper we focus on the results of ab initio calculations of their structural, electronic, optical, elastic and thermal properties within the density functional theory.

The outline of the paper is as follows. In section II we have given a brief review of the computational scheme used. The calculations of the structural, electronic and optical properties along with the computed elastic and thermal properties are described in section III; while the summary and conclusions are drawn in section VI.

2. Computational method

The calculations were done using FP-LAPW computational scheme [10,11] as implemented in the WIEN2K code [12]. The FP-LAPW method expands the Kohn-Sham orbitals in atomic like orbitals inside the muffin-tin (MT) atomic spheres and plane waves in the interstitial region. The Kohn-Sham equations were solved using the recently developed Wu-Cohen generalized gradient approximation (WC-GGA) [13, 14] for the exchange-correlation (XC) potential. It has been shown that this new functional is more accurate for solids than any existing GGA and meta-GGA forms. For a variety of materials, it improves the equilibrium lattice constants and bulk moduli significantly over local-density approximation [15] and Perdew-Burke-Ernzerhof (PBE) [16] and therefore is a better choice. For this reason we adopted the new WC approximation for the XC potential in studying the present systems. Further for electronic structure calculations modified Becke–Johnson potential (mBJ) [17] as coupled with WC-GGA is used.

The valence wave functions inside the atomic spheres were expanded up to $l=10$ partial waves. In the interstitial region, a plane wave expansion with $R_{MT}K_{max}$ equal to seven was used for all the investigated systems, where R_{MT} is the minimum radius of the muffin-tin spheres and K_{max} gives the magnitude of the largest K vector in the plane wave expansion. The potential and the charge density were Fourier expanded up to $G_{max} = 10$. We carried out convergence tests for the charge-density Fourier expansion using higher G_{max} values. The R_{MT} (muffin-tin radii) are taken to be 2.2, 2.3, 1.8, 2.0 and 2.19 atomic unit (a.u.) for Cu, Tl, S, Se and Te respectively. The modified tetrahedron method [18] was applied to integrate inside the Brillouin zone (BZ) with a dense mesh of 5000 uniformly distributed k-points (equivalent to 405 in irreducible BZ) where the total energy converges to less than 10^{-6} Ry.

3. Results and discussion

3.1. Structural properties
The ternary chalcopyrite semiconductor crystallizes in the chalcopyrite structure with space group $I-\overline{4}2d$ (D_{2d}^{12}). The Cu atom is located at (0,0,0); (0,1/2,1/4), Ga at (1/2,1/2,0); (1/2,0,1/4) and X at (u,1/4,1/8); (-u,3/4,1/8); (3/4,u,7/8); (1/4,-u,7/8). Two unequal bond lengths d_{Cu-X} and d_{Tl-X} result in two structural deformations, first is characterized by u parameter defined as $u=0.25+ (d_{Cu-X}^2 - d_{Tl-X}^2)/a^2$ where a is the lattice parameter in x and y direction, and the second parameter $\eta=c/a$, where c is lattice parameter in z direction which is generally different from 2a.

To determine the best energy as a function of volume, we minimized the total energy of the system with respect to the other geometrical parameters. The minimization is done in two steps, first parameter u is minimized by the calculation of the internal forces acting on the atoms within the unit cell until the forces become negligible, for this MINI task is used which is included in the WIEN2K code. Second, the total energy of crystal is calculated for a grid of volume of the unit cell (V) and c/a values, where each point in the grid involves the minimization with respect to u.

Five values of c/a are used for each volume and a polynomial is then fitted to the calculated energies to calculate the best c/a ratio. The result is an optimal curve (c/a, u) as a function of volume. Further a final optimal curve of total energy is obtained by minimize energy verses [V, c/a (V), u (V)] by FPLAPW calculations and Murnaghan equation of state [19].

Further we have used the calculated lattice constants for determination of inter atomic distance for A – C and B – C bonds by the following relations [8].

$$x = 0.5 - (c^2 / 32\ a^2\ -\ 1/16\ )^{1/2}; \qquad d_{A\text{-}C} = [a^2 x^2 + (4a^2 + c^2)\ /\ 64]^{1/2};$$

$$d_{B\text{-}C} = [a^2(1/2 - x)^2 + (4a^2 + c^2)\ /\ 64]^{1/2}; d\ (\text{in Å}) = (d_{A\text{-}C} + d_{B\text{-}C})/2 \qquad (1)$$

We have also calculated the bulk modulus (B in GPa)by using the semi-empirical equation developed by Verma et al [20] for chalcopyrite semiconductors as follows,

$$B = 4056\,(Z_1 Z_2 Z_3)^{0.15}\,d^{-5} \qquad (2)$$

where d is the inter atomic distance and $Z_1 Z_2 Z_3$ (product of ionic charges)= 12 for $A^I B^{III} C_2^{VI}$ semiconductors. Table 1 presents the lattice constants and obtained along with the bulk modulus and its pressure derivative.

3.2. Electronic and optical properties

Fig.1 shows the band structures of the $CuTlS_2$, $CuTlSe_2$ and $CuTlTe_2$. The calculations show that these compounds have semiconducting nature with the direct band gap of 0.113 eV, 0.029 eV and 0.177 eV for $CuTlS_2$, $CuTlSe_2$ and $CuTlTe_2$respectively.As clear from the figure 1 for the band structure that the obtained electronic band gap is lower than the values predicted by experiments. Also because of the lack of the data available we are not able to compare the values obtained for $CuTlSe_2$ and $CuTlTe_2$. Deshpande et al, [21, 22] reported an estimate of the band gap of $CuTlS_2$ by X-ray spectroscopic study. V. Estrella et al, [23] prepared the tetragonal $CuTlS_2$ by chemical bath method at 300 °C, the band gap found was 1.25 eV.
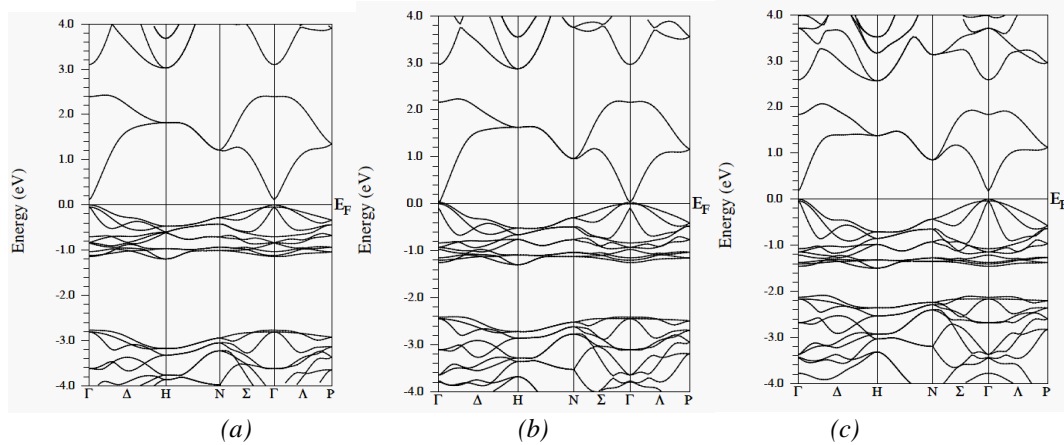

Fig. 1. Band structures of (a) CuTlS₂, (b) CuTlSe₂ and (c) CuTlTe₂.

To describe the general features of bonding in more detail the partial and total density for states (PDOS and DOS) for copper thallium dichalcogenides are calculated using the mBJ potential together with WC-GGA for the correlation (Fig.2). The upper valence band mainly consists of Cu 3d-states with a few contribution of X (X=S, Se and Te) p-states. The conduction bands near Fermi level are composed of strongly hybridized Tl 6s and X (X=S, Se and Te) p-states.
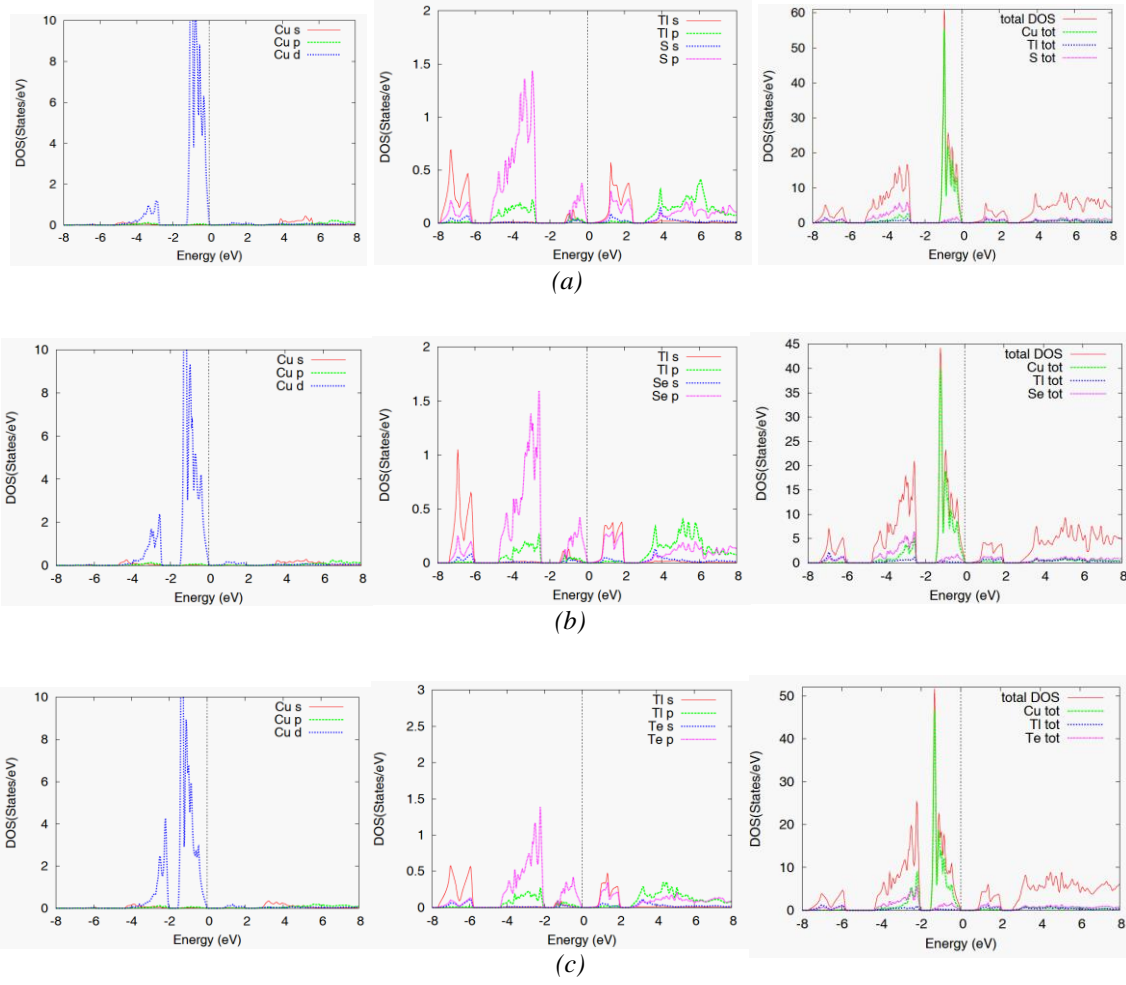
Fig. 2. The calculated partial and total density of states (DOS) for (a) CuTlS$_2$,
(b) CuTlSe$_2$ and (c) CuTlTe$_2$.

The linear response to an external electromagnetic field with a small wave vector is measured through the complex dielectric function,

$$\varepsilon(\omega)= \varepsilon_1(\omega)+ i\varepsilon_2(\omega) \qquad (3)$$

which is related to the interaction of photons with electrons[24]. The imaginary part $\varepsilon_2(\omega)$ of the dielectric function could be obtained from the momentum matrix elements between the occupied and unoccupied wave functions and is given by [25]

$$\varepsilon_2(\omega) = \frac{2\pi^2 e^2}{\Omega\varepsilon_0} \sum_{i\in c.f\in v} \sum_{k} \left| \left\langle \Psi_k^c \left| \hat{\mu}.r \right| \Psi_k^v \right\rangle \right|^2 \delta\left[E_k^c - E_k^v - \hbar\omega \right] \qquad (4)$$

The real part $\varepsilon_1(\omega)$ can be evaluated from $\varepsilon_2(\omega)$ using the Kramer-Kronig relations and is given by[26]

$$\varepsilon_1(\omega) = 1 + \left(\frac{2}{\pi}\right) \int_0^\infty \frac{\omega'^2 \varepsilon_2(\omega')}{\omega'^2 - \omega^2} d\omega'. \qquad (5)$$

All of the other optical properties, including the absorption coefficient $\alpha(x)$, the refractive index $n(x)$, the extinction coefficient $k(x)$, and the energy-loss spectrum $L(x)$, can be directly calculated from $\varepsilon_1(\omega)$ and $\varepsilon_2(\omega)$[25,27].

Fig.3 displays the real and imaginary parts of the electronic dielectric function $\varepsilon(\omega)$ spectrum for the photon energy ranging up to 40 eV, respectively. As it clear from the optical spectra of real part of the electronic dielectric function $\varepsilon_1(\omega)$ exhibit anisotropy in the different directions (along basal-plane and z-axis) with a very small difference (0.0246, 0.2484 and 0.2407 eV for $CuTlS_2$, $CuTlSe_2$ and $CuTlTe_2$ respectively) in the static limit. The imaginary part of the dielectric constant $\varepsilon_2(\omega)$ is the fundamental factor of the optical properties of a material. Fig.3 displays the imaginary (absorptive) part of the dielectric function $\varepsilon_2(\omega)$ up to 40 eV.
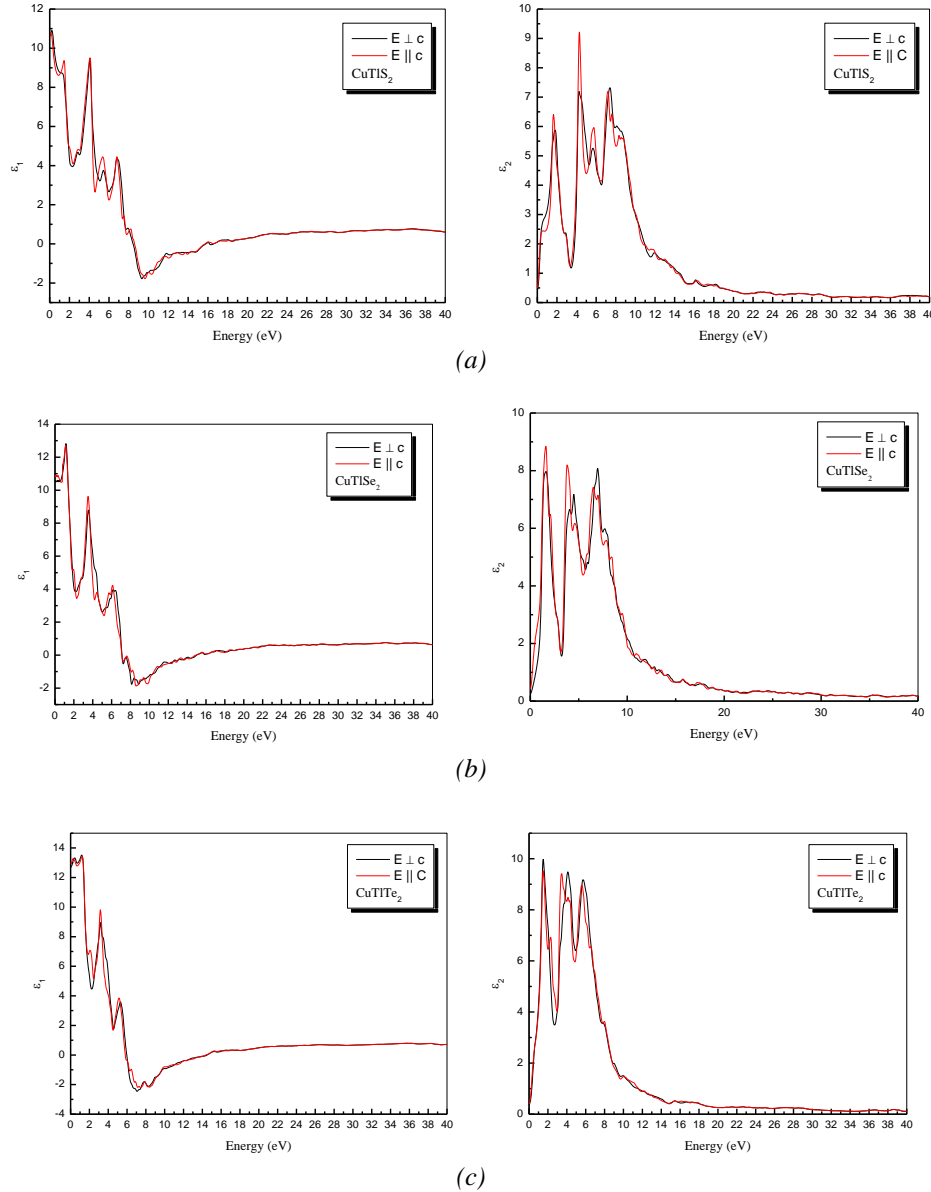

Fig. 3. The calculated real $\varepsilon_1(\omega)$ and imaginary $\varepsilon_2(\omega)$ parts of complex dielectric constant for (a) $CuTlS_2$, (b) $CuTlSe_2$ and (c) $CuTlTe_2$.

Fig.4 presents the refractive index n (ω) along with the extinction coefficient k (ω). The refractive index spectrum shows an anisotropic behavior (Δn(0 eV)=0.00406, 0.17586, 0.0337 for $CuTlS_2$, $CuTlSe_2$ and $CuTlTe_2$, respectively)hence only the averages are listed in Table 2.Fig.4 also show extinction coefficient k (ω) is related to the decay or damping of the oscillation

amplitude of the incident electric field, the extinction coefficient k (ω) decreases with increasing the incident photon energy. The refractive index and extinction coefficient both oscillate for all chosen materials.

Table 2. The calculated minimum refractive index (n) and dielectric constant for CuTlS$_2$, CuTlSe$_2$ and CuTlTe$_2$ compared with other experimental and theoretical data.

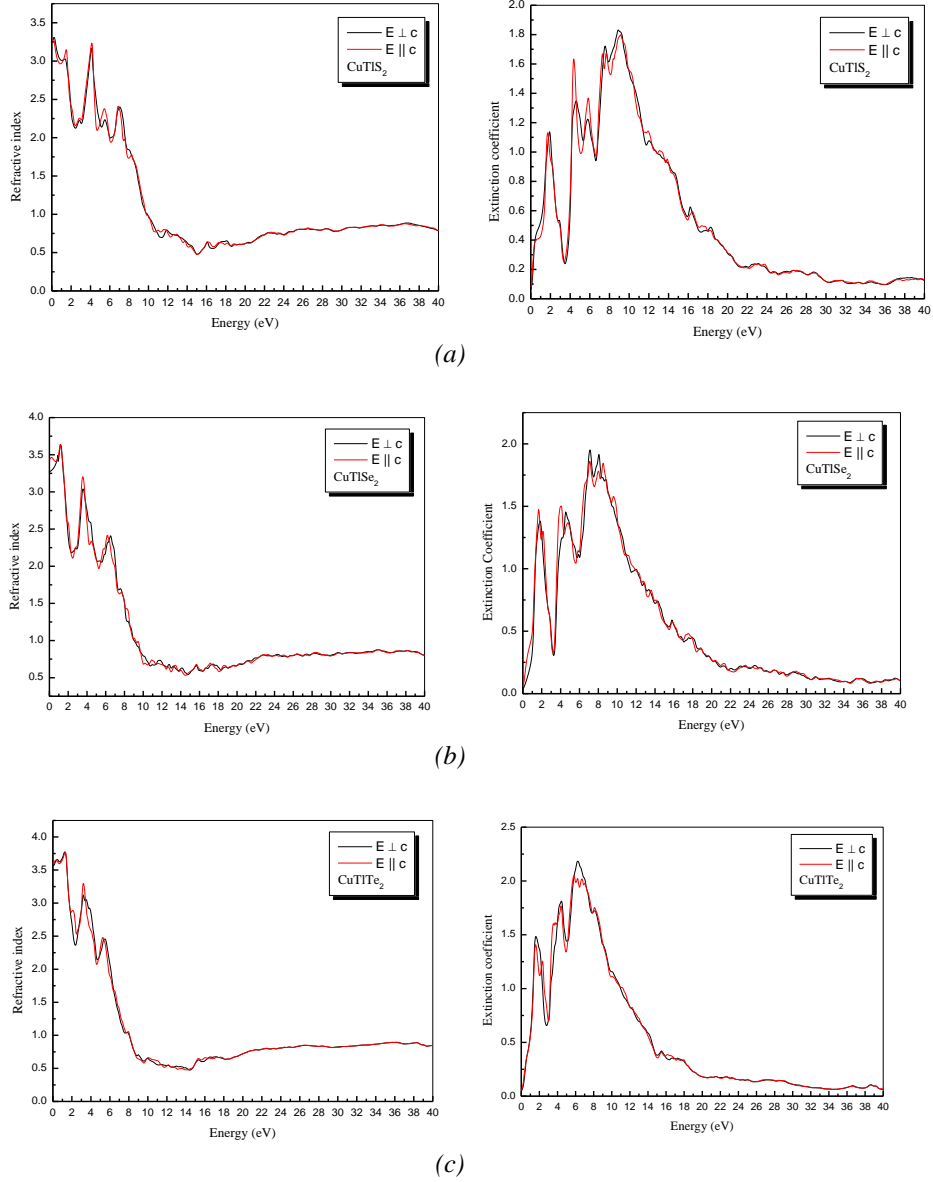| Crystals	n calculated (eq. 6)	n this work	ε_∞ this work
CuTlS$_2$	2.736	3.26	10.6
CuTlSe$_2$	3.000	3.30	10.9
CuTlTe$_2$	3.404	3.58	12.8

(a)

(b)

(c)

Fig. 4. The calculated refractive index and extinction coefficient for (a) CuTlS$_2$, (b) CuTlSe$_2$ and (c) CuTlTe$_2$.

The refractive index (n) of these compounds can also be evaluated by using the relation given by Verma et al [28] for chalcopyrites as follows,

$$n = 0.31(Z_1 Z_2 Z_3)^{0.15} d^2 \qquad (6)$$

Where d is the inter atomic distance and $Z_1 Z_2 Z_3$ (product of ionic charges) =12 for $A^I B^{III} C_2^{VI}$ semiconductors.

The calculated optical reflectivity R (ω) is displayed in Fig.5. The maximum reflectivity occurs in ultra-violet region, 7.58-11.49 eV for $CuTlS_2$, 6.76-10.84 eV for $CuTlSe_2$ and 5.78-9.78 eV for $CuTlTe_2$. Also, the positions of the peaks also shift to lower energy regions while moving from S to Te.
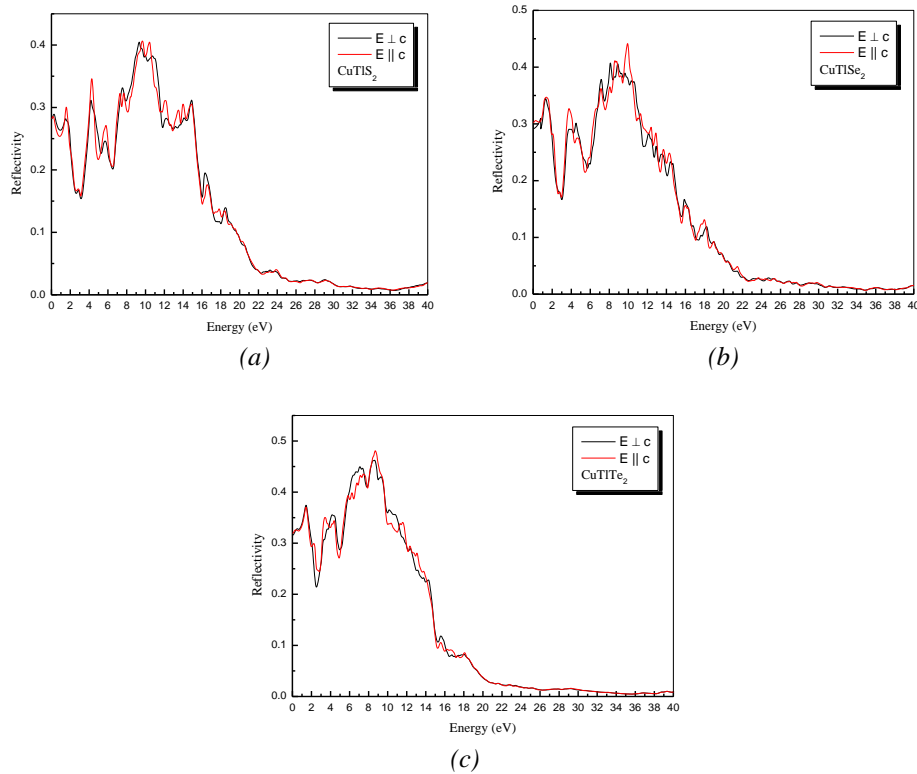

(a)

(b)

(c)

Fig. 5. The calculated reflectivity (R (ω)) for (a) CuTlS$_2$, (b) CuTlSe$_2$ and (c) CuTlTe$_2$.

Optical conductivity parameters are closely related to the photo-electric conversion efficiency and mainly used to measure the change caused by the illumination. Fig.6 shows the optical conductivities of $CuTlS_2$, $CuTlSe_2$ and $CuTlTe_2$ respectively. It's clear that these materials have a small values of conductivity in the visible light region (1.65 eV-3.1 eV), but have high values in the ultra violet region.
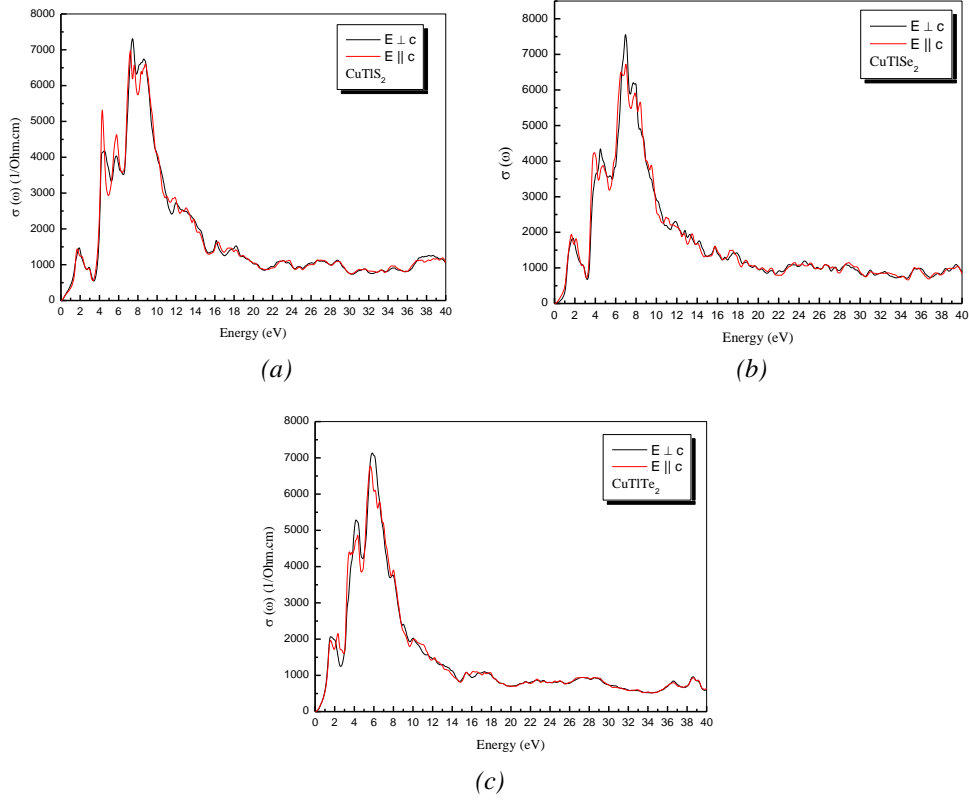
(a)

(b)

(c)

Fig. 6. The calculated photoconductivity ($\sigma(\omega)$)for (a) CuTlS$_2$, (b) CuTlSe$_2$ and (c) CuTlTe$_2$.

3.3. Elastic properties

The elastic properties of a solid are among the most fundamental properties that can be predicted from the first-principles ground-state total-energy calculations. The determination of the elastic constants requires knowledge of the curvature of the energy curve as a function of strain for selected deformations of the unit cell. The deformations [29] are shown in Table 3 and chosen such that the strained systems have the maximum possible symmetry. The system has been optimized for each deformed cell geometry. The WIEN2K package [12] facilitates this task by providing a force-driven optimization of the internal cell geometry. The elastic stiffness tensor of chalcopyrite compounds has six independent components because of the symmetry properties of the D_{2d}^{12} space group, namely C$_{11}$, C$_{12}$, C$_{13}$, C$_{33}$, C$_{44}$ and C$_{66}$ in Young notation. The calculated elastic constant for the tetragonal phase of Cu-chalcopyrite's are listed in Table 4& 5. In general, our results are in good agreement with the experimental data, in particular if we consider, shear constants (C$_{44}$ and C$_{66}$) appear to be no worse than the rest of the elastic constants, even though the inner strain component is particularly difficult in those constants. The comparison with other theoretical calculations also shows an important dispersion of values. The calculated elastic constants fulfill the mechanical stability criteria for the tetragonal systems:

$$C_{11} > |C_{12}|, (C_{11}+C_{12})\, C_{33} > 2C_{13}^2, C_{44} > 0, \text{ and } C_{66} > 0$$

In order to check the internal consistency of calculated elastic constants we can compare the bulk modulus reported on Table 1 with an equivalent combination of the C$_{ij}$'s.

Table 1. Structural equilibrium parameters, a, c, u, d, B and B′ calculated in WC-GGA.

Crystals	a (Å)	c (Å)	u	d (Å) Eq. (1)	B (GPa)	B′
CuTlS$_2$	5.694, 5.58[a]	11.38, 11.16[a]	0.250	2.466	62, 65[b]	5.46
CuTlSe$_2$	5.950, 5.83[a]	11.97, 11.6[a]	0.246	2.582	52, 51[b]	5.02
CuTlTe$_2$	6.368	12.63	0.254	2.750	44, 37[b]	5.19

[a]Reference [8]; [b] equation (2)

Table 3. The lattice parameters of the deformed tetragonal unit cell, the expression relating the δ and ε variables, the finite Lagrangian strain tensor (Voigt notation) and the value of the second derivative, $(1/2V)(d^2E/d\varepsilon^2)$, in terms of the elastic constants (ε being deformation coordinate and E the energy).

Strained cell	ε	Strain (η)	$dE^2/d\varepsilon^2$
$(a+\delta, a+\delta, \dfrac{c+c\delta}{a}, 90,90,90)$	$\dfrac{(a+\delta)^2}{a^2}-1$	$(\dfrac{\varepsilon}{2},\dfrac{\varepsilon}{2},\dfrac{c\varepsilon}{2a},0,0,0)$	$\dfrac{1}{4}(C_{11}+C_{12})+\dfrac{1}{8}C_{33}+\dfrac{1}{2}C_{13}$
$(a+\delta, a+\delta, c, 90,90,90)$	$\dfrac{(a+\delta)^2}{a^2}-1$	$(\dfrac{\varepsilon}{2},\dfrac{\varepsilon}{2},0,0,0,0)$	$\dfrac{1}{4}(C_{11}+C_{12})$
$(a, a, \dfrac{c+c\delta}{a}, 90,90,90)$	$\dfrac{(c+\delta)^2}{c^2}-1$	$(0,0,\dfrac{\varepsilon}{2},0,0,0)$	$\dfrac{1}{8}C_{33}$
$(a, a+\delta, c, 90,90,90)$	$\dfrac{(a+\delta)^2}{a^2}-1$	$(0,\dfrac{\varepsilon}{2},0,0,0,0)$	$\dfrac{1}{8}C_{11}$
$(a, a, c, 90,90+\delta,90)$	$\sin\delta$	$(0,0,0,0,\varepsilon,0)$	C_{44}
$(a, a, c, 90,90,90+\delta)$	$\sin\delta$	$(0,0,0,0,0,\varepsilon)$	C_{66}

Table 4. Elastic constants C$_{ij}$ (in GPa) of the Cu-chalcopyrites compared with available data.

Solids	C$_{11}$	C$_{12}$	C$_{13}$	C$_{33}$	C$_{44}$	C$_{66}$
CuTlS$_2$	70.4	52.9	46.9	67.9	33.1	27.3
CuTlSe$_2$	60.8, 95[c]	40.9, 59.5[c]	44.0, 56.5[c]	70.9, 89.2[c]	24.4, 32.7[c]	23.2, 29.7[c]
CuTlTe$_2$	52.8	36.8	36.2	53.3	20.9	20.1

[c]equation (27).

Table 5. Elastic moduli of the Cu-chalcopyrites.

Solids	B (GPa)	G (GPa)	Y (GPa)	ν	κ$_a$ (GPa^{-1})	κ$_c$ (GPa^{-1})	B/G
CuTlS$_2$	56, 65[b]	20	53	0.34	0.0053	0.0074	2.68
CuTlSe$_2$	50, 51[b]	17	46	0.34	0.0081	0.0041	2.62
CuTlTe$_2$	35, 37[b]	16	43	0.29	0.0079	0.0080	2.36

[b] equation (2)

Bulk modulus should be bound from above by the Voigt approximation (uniform strain assumption) [30, 31]:

$$B_V = \frac{1}{9}(2C_{11}+C_{33}+2C_{12}+4C_{13}) \qquad (7)$$

Reuss found lower bounds for all lattices [32]

$$B_R = \frac{(C_{11} + C_{12})C_{33} - 2C_{13}^2}{C_{11} + C_{12} + 2C_{33} - 4C_{13}} \tag{8}$$

Voigt and Reuss approximations provide, in fact, an estimation of the elastic behaviour of an isotopic material, for instance a polycrystalline sample. Such a medium would have a single shear constant, G, upper bounded by

$$G_V = \frac{1}{30}(M + 3C_{11} - 3C_{12} + 12C_{44} + 6C_{66}) \tag{9}$$

and lower bounded by

$$G_R = 15\left\{\frac{18B_V}{C^2} + \frac{6}{(C_{11} - C_{12})} + \frac{6}{C_{44}} + \frac{3}{C_{66}}\right\}^{-1} \tag{10}$$

where $C^2 = (C_{11} + C_{12})C_{33} - 2C_{13}^2$

In the Voigt-Reuss-Hill approximation [33], the B and G of the polycrystalline material are approximated as the arithmetic mean of the Voigt and Reuss limits:

$$B = \frac{B_V + B_R}{2} \tag{11}$$

$$G = \frac{G_V + G_R}{2} \tag{12}$$

Finally the Poisson ratio and the Young modulus are obtained as

$$\upsilon = \frac{3B - 2G}{2(3B + G)} \tag{13}$$

$$Y = \frac{9BG}{3B + G} \tag{14}$$

Using the single crystal C_{ij} data, one can evaluate the linear compressibilities along the principles axis of the lattice. For the tetragonal structure, the linear compressibilities κ_a and κ_c along the a- and c-axis respectively are given in term of elastic constants by the following relations;

$$\kappa_a = -\frac{1}{a}\frac{\partial a}{\partial p} = \frac{C_{33} - C_{13}}{C_{33}(C_{11} + C_{12}) - 2C_{13}^2} \tag{15}$$

$$\kappa_c = -\frac{1}{c}\frac{\partial c}{\partial p} = \frac{C_{11} + C_{12} - 2C_{13}}{C_{33}(C_{11} + C_{12}) - 2C_{13}^2} \tag{16}$$

Pugh [34] proposed that the resistance to plastic deformation is related to the product Gb, where 'b' is the Burgers vector, and that the fracture strength is proportional to the product Ba, where 'a' corresponds to the lattice parameter. As b and a are constants for specific materials, the Ba/Gb can be simplified into B/G. This formula was recently exploited in the study of brittle vs

ductile transition in intermetallic compounds from first-principles calculations [35, 36]. A high B/G ratio is associated with ductility, whereas a low value corresponds to the brittle nature. The critical value which separates ductile and brittle material is around 1.75, i.e., if B/G > 1.75, the material behaves in a ductile manner otherwise the material behaves in a brittle manner. We have found that B/G ratios are 2.80, 2.88 and 2.10 for CuTlS$_2$, CuTlSe$_2$ and CuTlTe$_2$ respectively, classifying these materials as ductile. Consequently, the Ba/Gb reflects the competition between the shear and cohesive strengths at the crack tip of fracture.

3.4. Thermal properties

To investigate the thermodynamic properties of Cu-chalcopyrite, we have used Gibbs program. The obtained set of total energy versus primitive cell volume determined in previous section has been used to derive the macroscopic properties as a function of temperature and pressure from the standard thermodynamic relations. Gibbs program is based on the quasi-harmonic Debye model [37], in which the non-equilibrium Gibbs function G*(V; P, T) can be written in the form of:

$$G^*(V;P,T) = E(V) + PV + A_{vib}[\theta_D;T]$$

(17)

where E(V) is the total energy per unit cell, PV corresponds to the constant hydrostatic pressure condition, θ_D is the Debye temperature, and A$_{vib}$ is the vibrational term, which can be written using the Debye model of the phonon density of states as [38,39]:

$$A_{vib}[\theta_D;T] = nkT\left[\frac{9\theta}{8T} + 3\ln(1 - e^{-\theta/T}) - D\left(\frac{\theta}{T}\right)\right]$$

(18)

where n is the number of atoms per formula unit, D(θ/T) represents the Debye integral, and for an isotropic solid, θ is expressed as [38]:

$$\theta_D = \frac{\hbar}{k}\left[6\pi^2 V^{1/2} n\right]^{1/3} f(\sigma)\sqrt{\frac{B_S}{M}}$$

(19)

M being the molecular mass per unit cell and B$_S$ the adiabatic bulk modulus, approximated by the static compressibility [37]:

$$B_S \cong B(V) = V\frac{d^2 E(V)}{dV^2}$$

(20)

$f(\sigma)$ is given by Refs. [37,40, 41]; where σ is the Poisson ratio.

Therefore, the non-equilibrium Gibbs function G*(V; P, T) as a function of (V; P, T) can be minimized with respect to volume V,

$$\left(\frac{\partial G^*(V;P,T)}{\partial V}\right)_{P,T} = 0$$

(21)

By solving Eq. (21), one can obtain the thermal equation of state (EOS) V(P, T). The heat capacity C$_V$ and the thermal expansion coefficient α are given by [33],

$$C_V = 3nk\left[4D\left(\frac{\theta}{T}\right) - \frac{3\theta/T}{e^{\theta/T} - 1}\right]$$

(22)

$$S = nk\left[4D\left(\frac{\theta}{T}\right) - 3\ln(1 - e^{-\theta/T})\right]$$

(23)

$$\alpha = \frac{\gamma C_V}{B_T V}$$

(24)

where γ is the Grüneisen parameter, which is defined as:

$$\gamma = -\frac{d \ln \theta(V)}{d \ln V}$$

(25)

Through the quasi-harmonic Debye model, one could calculate the thermodynamic quantities of any temperatures and pressures of compounds from the calculated E–V data at T = 0 and P = 0.

We can also provide a prediction of the hardness (H in GPa) and six independent elastic constants (C_{ij} in GPa)by using the semi-empirical equations developed by Verma and co-authors[20, 42],

$$H = K\, B^{K+1}$$

(26)

B = Bulk modulus; K = 0.5 for $A^{I}B^{III}C_2^{VI}$

$$C_{ij} = A_{ij} \times \left(\frac{k_B T_m}{(Z_1 Z_2 Z_3)\Omega}\right)^{0.15} \quad (i = 1, 3, 4, 6 \text{ and } j = 1, 2, 3, 4, 6)$$

(27)

$A_{11} = 160$, $A_{12} = 100$, $A_{13} = 95$, $A_{33} = 150$, $A_{44} = 55$, $A_{66} = 50$

where Z_1, Z_2 and Z_3 are the ionic charges on the A, B and C_2, respectively and the value of product of ionic charge is 12 for $A^{I}B^{III}C_2^{VI}$ [42].

As the melting point of $CuTlSe_2$ is 678 K [8] so the temperature range from 0 K to 800 K for $CuTlS_2$, 0 K to 600 K for $CuTlSe_2$ and 0 to 500 K for $CuTlTe_2$ have been taken to determine the thermodynamic properties through the quasi-harmonic Debye model. The pressure effects are studied in the 0–8GPa range. Fig.7 presents relationships between the equilibrium volume V (bohr^3) and pressure at various temperatures. Meanwhile, V increases slightly as the temperature increases, whereas the equilibrium volume V decreases dramatically as the pressure P increases at a given temperature. This account suggests that the $CuTlX_2$ (X= S, Se, Te) under loads turns to be more compressible with increasing pressure than decreases temperature. Furthermore, It is noted that the relationship between the bulk modulus and temperature for $CuTlX_2$ (X= S, Se, Te) in Fig.8. The bulk modulus slightly decreases with increasing temperature at a given pressure and increases with increasing pressure at a given temperature.
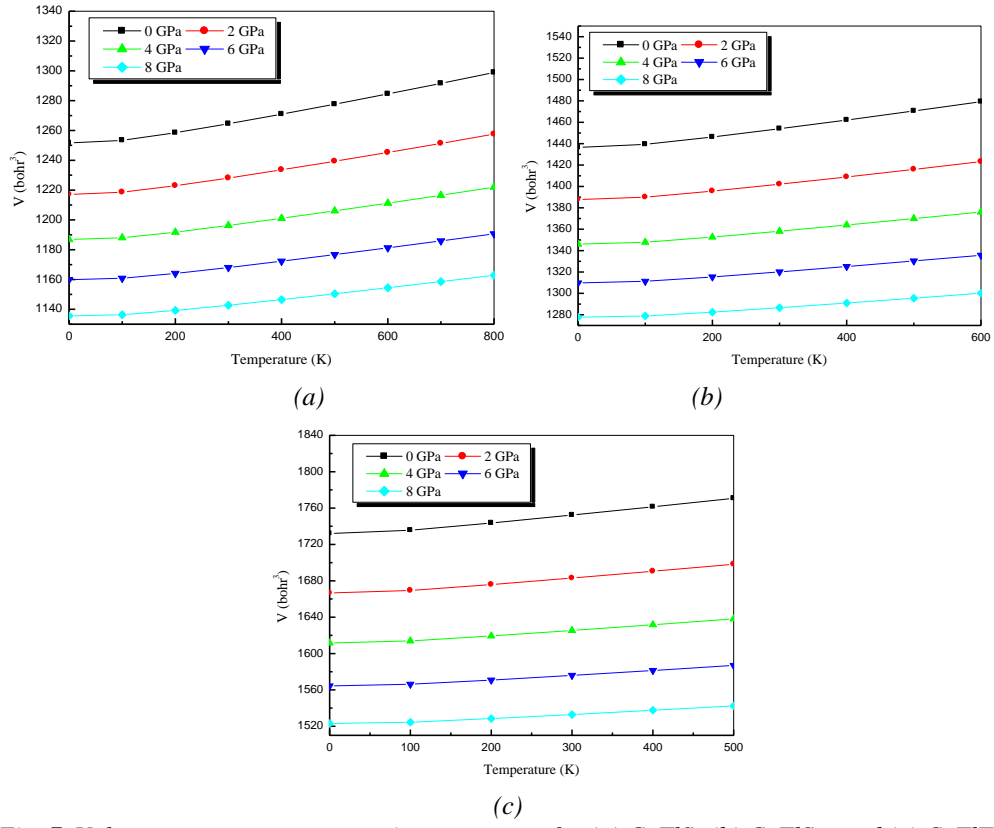
(a) *(b)*

(c)

Fig. 7. Volume vs temperature at various pressures for (a) CuTlS$_2$ (b) CuTlSe$_2$ and (c) CuTlTe$_2$.
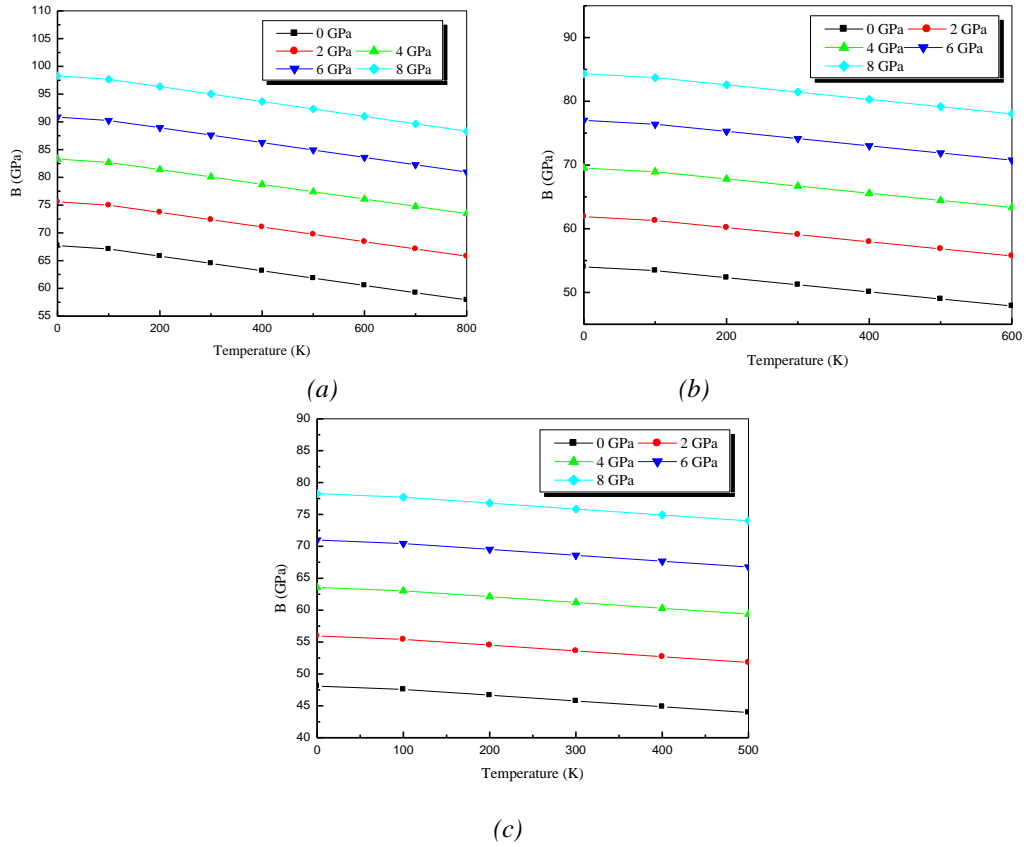

(a) *(b)*

(c)

Fig. 8. Bulk modulus vs temperature at various pressures for (a) CuTlS$_2$ (b) CuTlSe$_2$ and (c) CuTlTe$_2$.

The variation of the Debye temperature θ_D (K) as a function of pressure and temperature illustrated by our results is displayed in Fig.9. With the applied pressure increasing, the Debye temperatures are almost linearly increasing. Fig.10 shows the volume thermal expansion coefficient $\alpha(10^{-5}/K)$ of CuTlX$_2$ (X= S, Se, Te) at various pressures, from which it can be seen that the volume thermal expansion coefficient α increases quickly at a given temperature particularly at zero pressure below the temperature of 300 K. After a sharp increase, the volume thermal expansion coefficient of the CuTlX$_2$ (X= S, Se, Te) is nearly insensitive to the temperature above 300 K due to the electronic contributions.
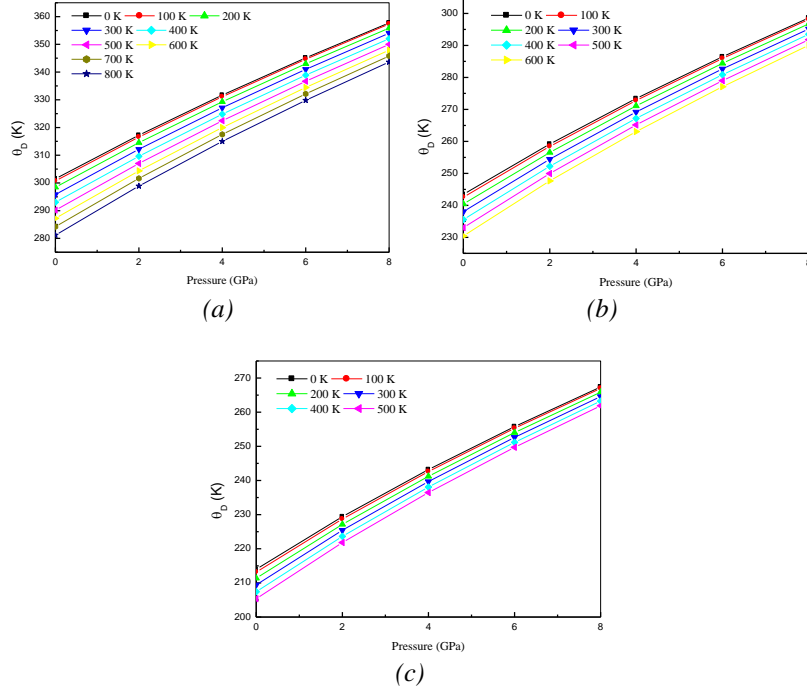
*Fig. 9. Debye temperature vs pressure at various temperatures for (a) CuTlS$_2$
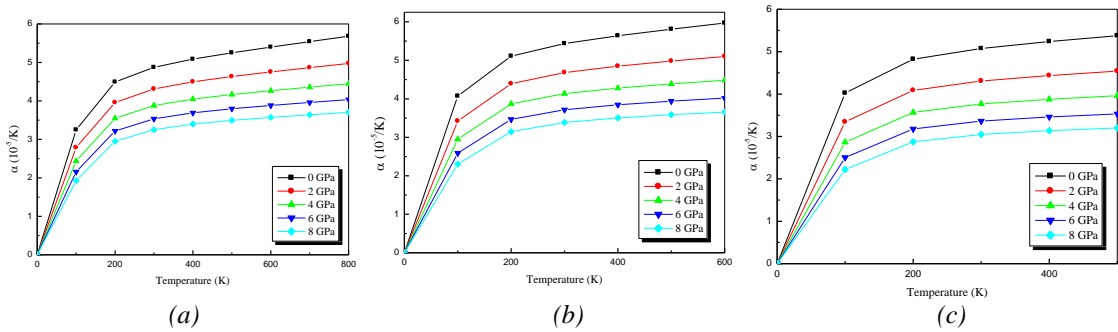(b) CuTlSe$_2$ and (c) CuTlTe$_2$.*

*Fig. 10. Thermal expansion coefficients vs temperature at various pressures for
(a) CuTlS$_2$ (b) CuTlSe$_2$ and (c) CuTlTe$_2$.*

As very important parameters, the heat capacities of a substance not only provide essential insight into the vibrational properties but are also mandatory for many applications. Our calculation of the heat capacities C_P and C_V of CuTlS$_2$, CuTlSe$_2$ and CuTlTe$_2$ verses temperature at pressure range 0-8GPa are shown in the following Figs.11 to13 respectively. From these figures, we can see that the constant volume heat capacity C_V and the constant pressure capacity C_P are very similar in appearance and both of them are proportional to T^3 at low temperatures. At high

temperatures, the anharmonic effect on heat capacity is suppressed; which is called Dulong-Petit limit, with the increasing of the temperature, whereas C_P increases monotonically with the temperature. Fig.14 shows the entropy vs temperature at various pressures for $CuTlX_2$ (X= S, Se, Te). The entropies are variable by power exponent with increasing temperature but the entropies are higher at low pressure than that at high pressure at same temperature. The Gruneisen parameter γ is another important quantity for the materials. In Fig.15, we have shown the values of Gruneisen parameter γ at different temperatures and pressures. It shows the value γ increases as the temperature increases at a given pressure and decreases as the pressure increases at a given temperature.
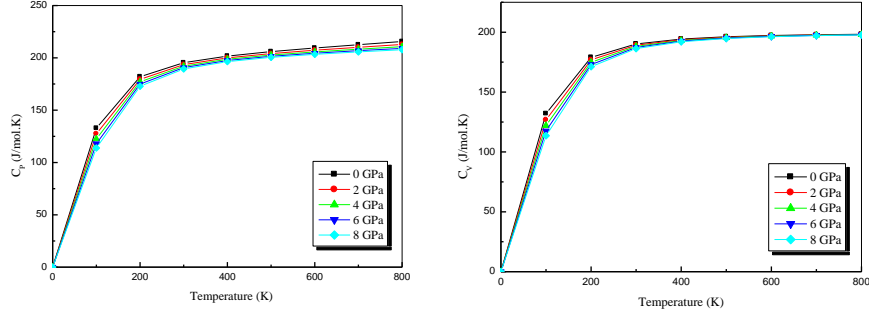

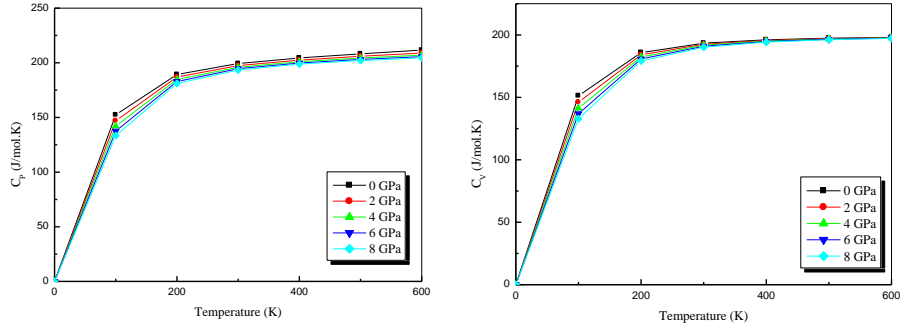Fig. 11. Heat capacity vs temperature at various pressures for $CuTlS_2$.

Fig. 12. Heat capacity vs temperature at various pressures for $CuTlSe_2$.
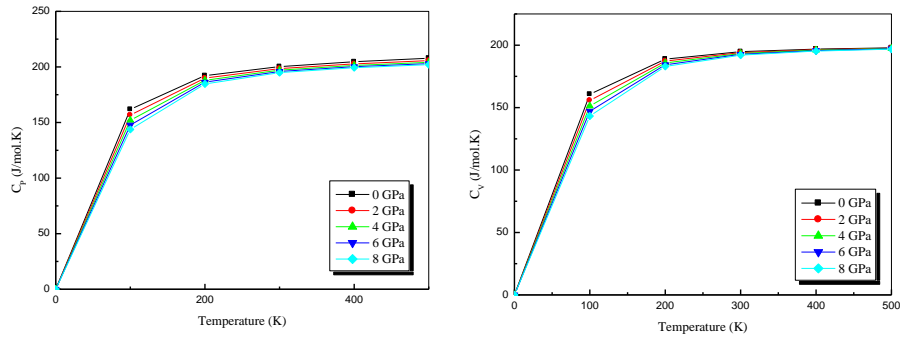

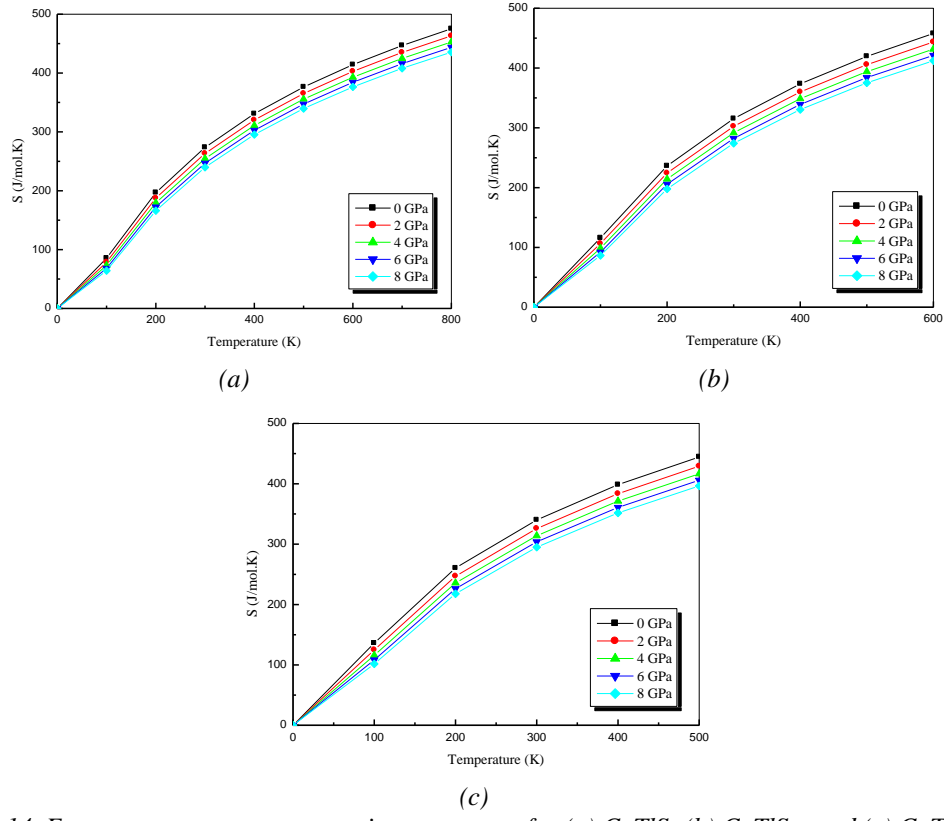Fig. 13. Heat capacity vs temperature at various pressures for $CuTlTe_2$.

(a)

(b)

(c)

Fig. 14. Entropy vs temperature at various pressures for (a) CuTlS₂ (b) CuTlSe₂ and (c) CuTlTe₂.

(a)

(b)

(c)
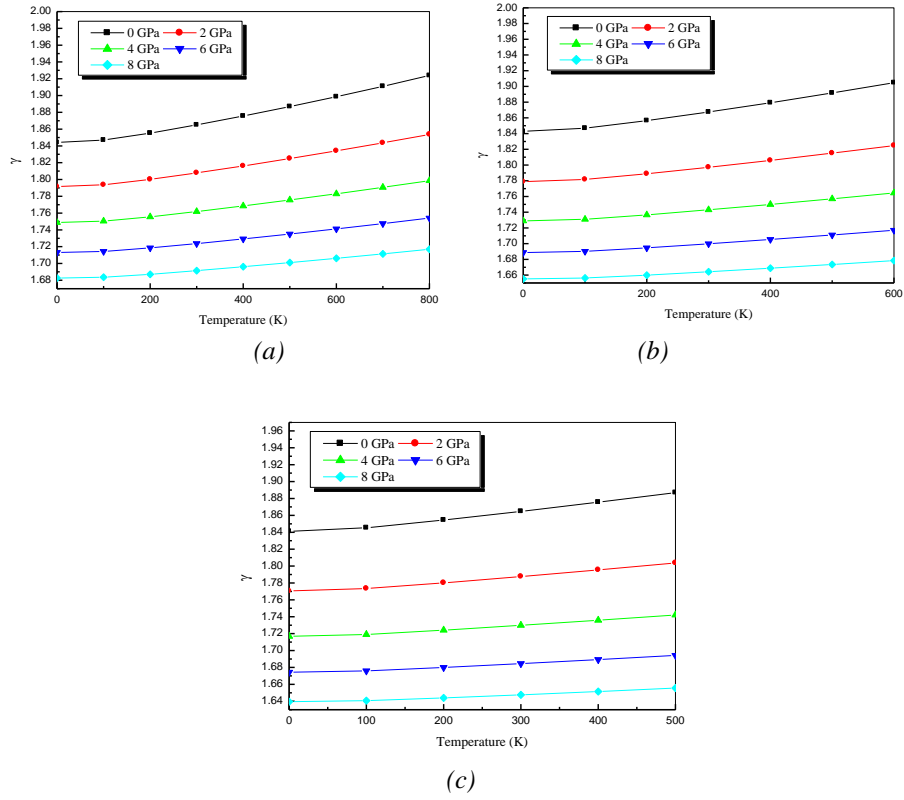
Fig. 15. Gruneisen parameter vs temperature at various pressures for (a) CuTlS₂ (b) CuTlSe₂ and (c) CuTlTe₂.

In Fig.16, we have shown the values of hardness (H in GPa) at different temperatures and pressures. It shows the hardness decreases as the temperature increases at a given pressure and increases as the pressure increases at a given temperature. The values of hardness are reported for the first time at different pressure and temperature. Table 6 present the thermal properties such as isothermal bulk modulus, hardness, Gruneisen parameter, Debye temperature and thermal expansion coefficient at 300 K.

Table 6. Selection of thermal properties at 300 K; isothermal bulk modulus (B in GPa), Hardness (H in GPa), Gruneisen parameter (γ), Debye temperature (θ_D in K) and thermal expansion coefficient (α in 10^{-5}/K).

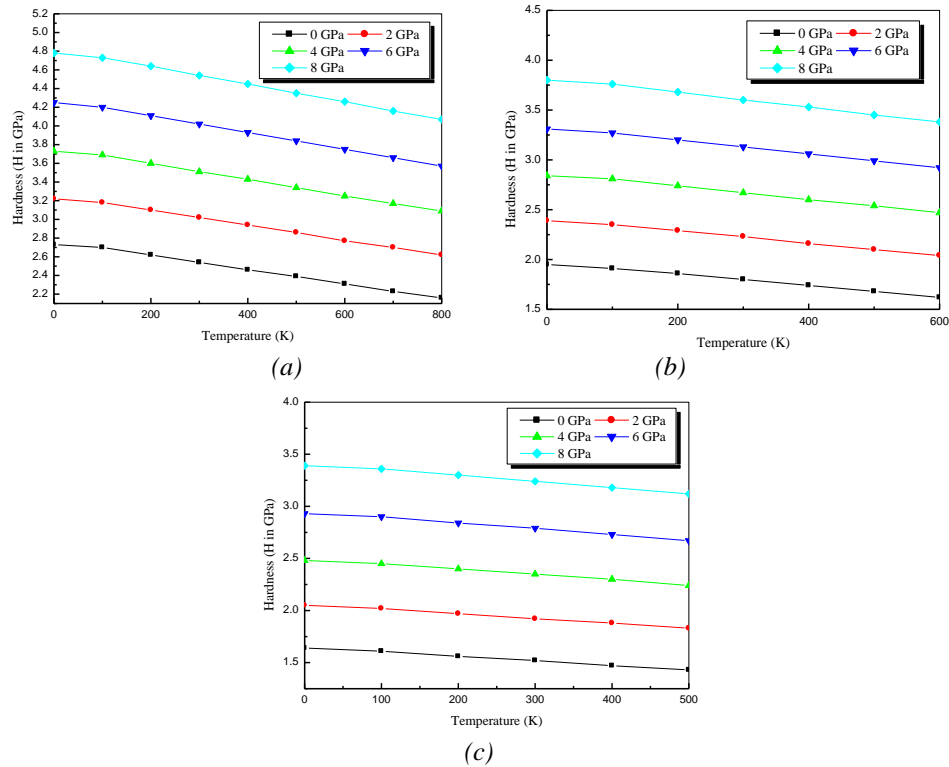| Solids	B (GPa)	H (GPa)	γ	θ_D (K)	α (10^{-5}/K)
$CuTlS_2$	65	2.54	1.86	295, 273[d]	4.87
$CuTlSe_2$	51	1.80	1.87	238, 230[d]	5.04
$CuTlTe_2$	46	1.52	1.87	209	5.10

[d]Reference [43]

(a)

(b)

(c)

*Fig. 16. Hardness vs temperature at various pressures for (a) CuTlS₂
(b) CuTlSe₂ and (c) CuTlTe₂.*

4. Conclusion

Employing the FP-LAPW approach based on density functional theory, within the WC-GGA as coupled with mBJ functional, we studied the structural, electronic, optical, elastic and thermal properties of the CuTlX₂ (X = S, Se and Te). All the considered semiconductors have a direct band gap (Γ-Γ). We compared electronic, optical and elastic properties with the available experiment and theoretical data. Thermal properties such as Gruneisen parameter, volume expansion coefficient, bulk modulus, specific heat, entropy, debye temperature and hardness are calculated successfully at various temperatures and pressures, and trends are discussed. To the best

of our knowledge, most of the investigated parameters are reported for the first time and hoped to stimulate the succeeding studies.

References

[1] V. L. Shaposhnikov, A. V. Krivosheeva, V. E. Borisenko, J. L. Lazzari, F. A. Avitaya, Phys. Rev. B **85**, 205201(1-9) (2012).
[2] Y. J. Dong, Y. L. Gao, Chalcogenide Letters **13**,515 (2016).
[3] A. K. Kushwaha, R. Khenata, A. Bouhemadou, S. Bin-Omran, K. Haddadi, J. Electronic Materials**46**, 4109 (2017).
[4] A. S. Verma,Sol. Stat. Comm. **149**, 1236 (2009).
[5] A. S. Verma, Phil. Mag. **89**, 183 (2009).
[6] A. S. Verma, D. Sharma,PhysicaScripta**76**,22 (2007).
[7] A. S. Verma, Mat. Chem. Phys. **139**, 256 (2013).
[8] J. L. Shay, J. H. Wernick, Ternary, chalcopyrite semiconductors: growth, electronic properties and application, Oxford: Pergamon Press,1975.
[9] J. Ruan, S. K. Jian, D. Zhang, H. Yao, H. Zhang, S. C. Zhang and D. Xing, Phys.Rev. Letts. **116**, 226801 (2016).
[10] G. K. H. Madsen, P. Blaha, K. Schwarz, E. Sjöstedt, L. Nordström, Phys. Rev. B **64**, 195134 (1-9) (2001).
[11] K. Schwarz, P. Blaha, G. K. H Madsen, Comput. Phys. Commun. **147**, 71 (2002).
[12] P. Blaha, K. Schwarz, G. K. H. Madsen, D. Kvasnicka, J. Luitz, WIEN2k: An Augmented Plane Wave+Local Orbitals Program for Calculating Crystal Properties, Karlheinz Schwarz/Techn. Universität Wien, Austria, 2001.
[13] Z. Wu, R. E. Cohen, Phys. Rev. B **73**, 235116 (1-6) (2006).
[14] F. Tran, R. Laskowski, P. Blaha, K. Schwarz, Phys. Rev. B **75**, 115131 (1-14) (2007).
[15] W. Kohn, L. J. Sham,Phys. Rev. **140**, A1133 (1965).
[16] J. P. Perdew, K. Burke, M. Ernzerhof, Phys. Rev. Lett. **77**, 3865 (1996).
[17] F. Tran, P. Blaha, Phys. Rev. Lett. **102**, 226401 (1-4) (2009).
[18] P. E. Blochl, O. Jepsen, O.K. Andersen, Phys. Rev. B **49**, 16223 (1994).
[19] F. D. Murnaghan, Proc. Natl. Acad. Sci. USA **30**,244 (1947).
[20] A. S. Verma, S. R. Bhardwaj, J. Phys: Condensed Matter **19**, 026213 (1-7) (2007).
[21] A. P. Deshpande, V. B. Sapre, C. Mande, J. Phys. C: Solid State Phys. **16**, L433 (1983).
[22] A. P. Deshpande, V. B. Sapre, C. Mande, J. Phys. C: Solid State Phys. **17**, 955 (1984).
[23] V. Estrella, R. Mejía, M.T. S. Nair, P.K. Nair,Mod. Phys. Lett. B **15**, 737 (2001).
[24] J. Sun, H. T. Wang, N. B. Ming, J. He, Y. Tian, Appl. Phys. Letts. **84**, 4544 (2004).
[25] S. Saha, T. P. Sinha,Phys. Rev. B **62**, 8828 (2000).
[26] P. Y. Yu, M. Cardona, Fundamentals of Semiconductors, Springer-Verlag, Berlin, 1996.
[27] M. Q. Cai, Z. Yin, M. S. Zhang,Appl. Phys. Letts **83**, 2805 (2003).
[28] A. S. Verma,Phys. Status Solidi B **246**, 192 (2009).
[29] J.F. Nye, Physical Properties of Crystals, Their Representation by Tensors andMatrices, Oxford Univ. Press, Oxford, USA, 1985.
[30] W. Voigt, Lehrbuch der Kristallphysik,Teubner, Leipzig, 1928.
[31] I. R. Shein, A.L. Ivanovskii, ScriptaMateriali**59**, 1099 (2008).
[32] A. Reuss, Z. Angew.Math. Mech. **9**, 49 (1929).
[33] R. Hill, Proc. Phys. Soc. Lond. **A 65**, 349 (1952).
[34] S. F. Pugh, Philos. Mag. **45**, 823 (1953).
[35] K. Chen, L. Zhao, J. S. Tse, J. Appl. Phys. **93**,2414 (2003).
[36] K. Chen, L. Zhao, J. S. Tse, Phys. Lett. A **331**, 400 (2004).
[37] M.A. Blanco, E. Francisco, V. Luaña, Comput. Phys. Commun. **158**, 57 (2004).
[38] M.A. Blanco, A. Martín Pendás, E. Francisco, J.M. Recio, R. Franco,J. Mol. Struct. Theochem. **368**,245 (1996).
[39] M. Flórez, J.M. Recio, E. Francisco, M.A. Blanco, A. Martín Pendás, Phys. Rev. B **66**,

144112 (1-8) (2002).

[40] E. Francisco, M.A. Blanco, G. Sanjurjo, Phys. Rev. B **63**, 094107 (1-9) (2001).

[41] J. P. Poirier, Introduction to the Physics of Earth's Interior, Cambridge University Press, Oxford, 2000, p. 39.

[42] A. S. Verma, S. Sharma, R. Bhandari, B. K. Sarkar, V. K. Jindal, Mat. Chem. and Phys. **132**, 416 (2012).

[43] V. Kumar, A. K. Shrivastava, R. Banerji, D. Dhirhe, Solid State Communications **149**, 1008 (2009).